Transport and Communications Science Journal, Vol. 77, Issue 7 (09/2026), 899-913

Transport and Communications Science Journal

DETERMINATION OF CONVECTIVE HEAT TRANSFER COEFFICIENT FOR THE INTERNAL SURFACES OF CONCRETE BOX GIRDERS USING COMPUTATIONAL FLUID DYNAMICS SIMULATION

Ngo Dang Quang, Bui Thi Thanh Mai*

University of Transport and Communications, No 3 Cau Giay Street, Hanoi, Vietnam

ARTICLE INFO

TYPE: Research Article
Received: 02/06/2026
Revised: 20/08/2026
Accepted: 07/09/2026
Published online: 15/09/2026
https://doi.org/10.47869/tcsj.77.7.2

* *Corresponding author*
Email: bttmai@utc.edu.vn; Tel: +84983525001

Abstract. The convective heat transfer coefficient (h_c) is a key parameter in heat transfer analysis and the thermal behavior of concrete structures. For the internal surfaces of enclosed structures, hc is typically determined under the assumption of zero air velocity. In the case of concrete box girders, empirical formulas have traditionally been used to estimate this coefficient. However, inside the box of a concrete box girder, temperature differences between the internal surfaces can drive air movement, which may affect hc. This paper presents the method and results of determining h_c for the internal surfaces of concrete box girder bridges using computational fluid dynamics (CFD) simulation, coupling fluid flow with heat transfer. The numerical model was validated against benchmark experimental data and field-measured temperatures from six full-scale bridge cross-sections. The results show that the average h_c ranges from approximately 3.71 to 4.90 $W \cdot m^{-2} \cdot K^{-1}$ and varies with cross-sectional geometry, rather than remaining constant as assumed in conventional empirical approaches. Smaller and more square-like sections generally exhibit higher h_c values. These findings provide more reliable reference values for thermal analysis of concrete box girder bridges.

Keywords: Convective heat transfer coefficient, internal surfaces, concrete box girders, computational fluid dynamics, heat transfer in fluids.

1. INTRODUCTION

In structures in general, and particularly in concrete box girder bridges, temperature distribution and especially temperature differences between different parts of the structure play an important role in their behavior. Thermal cracks have been found to be quite common in box girder bridges in many countries and Vietnam [1, 2].

Heat transfer occurs via three primary mechanisms: conduction, convection, and radiation. Convective heat transfer, which governs the exchange of thermal energy between a solid surface and the surrounding fluid medium (liquid or gas), plays a crucial role in the thermal behavior of concrete bridge structures. According to [3, 4], the heat flux attributed to convection can be three to four times greater than the heat transferred via long-wave radiation.

Mathematically, conductive heat transfer is governed by Fourier's law, which states that the heat flux (heat flow per unit area, q, in W/m²) is proportional to the negative temperature gradient:

$$q = -k\frac{dT}{dx} \tag{1}$$

where k is the thermal conductivity in W/(m·K) and $\frac{dT}{dx}$ is temperature gradient. This equation quantifies how heat diffuses through a material. For convective heat transfer between a surface and a moving fluid, Newton's law of cooling is used:

$$q_c = h_c\left(T_s - T_a\right) \tag{2}$$

where h_c is the convective heat transfer coefficient (W/m²·K), T_s is the surface temperature, and T_a is the fluid temperature far from the surface. Together, Fourier's law and Newton's law form the foundation for analyzing thermal behavior in engineering systems such as concrete box girder bridges.

The convective heat transfer coefficient (CHTC) is influenced by various factors - such as wind speed, surface roughness, color, porosity, and structural geometry - which affect local wind speed and turbulence intensity. Methods for determining CHTC generally fall into three categories: theoretical, experimental, and numerical. Each method has its own advantages and limitation [5]. Until now, in the engineering practice, the Kehlbeck's formula for h_c is widely applied [6]. This formula gives the empirical values of h_c for top, bottom, web and box inside surfaces. For inside surfaces h_c has a constant value

$$h_{c-in} = 3.5\left(W \cdot m^{-2} \cdot K^{-1}\right) \tag{3}$$

Based on measured temperature data in concrete and inverse problem solution, Ngo [7] demonstrated through inverse problem solutions that h_c for internal surfaces may vary between 3.9 and 5.5 $W \cdot m^{-2} \cdot K^{-1}$ depending on section geometry, suggesting that Kehlbeck's constant value is insufficient. However, the inverse approach requires dense thermocouple arrays embedded within the concrete cross-section, which is invasive and impractical for routine monitoring. Furthermore, it yields h_c as a back-calculated scalar without resolving the underlying airflow field, offering limited physical insight.

Currently, numerical methods integrating Computational Fluid Dynamics (CFD) with heat transfer analysis are widely used to determine CHTC, offering the distinct advantage of accurately simulating complex structural geometries. Numerous studies have applied CFD to determine convective heat transfer in buildings [8-10] and in closed cavity [11, 13]. However, the results of these studies cannot be applied to determine the CHTC of concrete bridge because of the differences in geometry configurations and temperature ranges. The coupled CFD and heat transfer framework presented in [5] was designed to calculate the h_c of the exterior surfaces of bridge girders, where airflow velocity and outer boundary configurations play a decisive role. Consequently, the findings from that study cannot be applied to determine the h_c of the inner cavity of box girders.

The present study addresses both limitations by applying CFD coupled with heat transfer, which directly resolves the buoyancy-driven airflow inside box girder and extracts h_c from the resulting near-wall thermal gradients. The only field measurements required are surface temperatures and the enclosed air temperature - quantities readily obtainable from surface-mounted sensors. Since there is minimal longitudinal air movement inside the bridge girder, this study focuses solely on the cross-sectional plane. Consequently, the simulation model is executed in 2D. The effect of longwave radiation is also neglected due to the relatively small clearance between the walls and the slabs.

The calculated convection heat transfer coefficient, h_c, across the investigated bridge cross-sections ranges from 3.9 to 4.9 $W/\left(m^2 \cdot K\right)$, which is slightly higher than the value recommended by Kehlbeck and consistent with the findings of Ngo. Furthermore, within the same bridge structure, h_c at smaller cross-sections tends to be higher than that at larger ones. For validation, these calculated hc values were utilized in long-term simulations of thermal distribution across the bridges, demonstrating high reliability.

2. METHODOLOGY

Based on [14], the convective heat transfer coefficient h_c at an interior concrete surface is derived from Eq.(2):

$$h_c = \frac{q_c}{T_s - T_a} \tag{4}$$

In analysis T_a is normally the bulk air temperature in the adjacent fluid domain, T_b. Determining h_c therefore reduces to an accurate evaluation of q_c, which, at a no-slip wall, is governed solely by molecular conduction across the vanishingly thin layer of stationary fluid in immediate contact with the surface:

$$q_c = -k_f \left(\frac{\partial T}{\partial n} \right)_{\text{wall}} \tag{5}$$

In this equation, k_f is the thermal conductivity of fluid. The central challenge then becomes resolving the near-wall temperature gradient $\partial T/\partial n$. This gradient is not a local property but is the footprint of the entire thermal and velocity field within the fluid domain, compressed into the wall-adjacent layer. Obtaining it requires solving the energy transport equation throughout the enclosed air volume:

$$\rho_f c_f\left(\frac{\partial T_f}{\partial t}+\mathbf{u}\cdot\nabla T_f\right)=\nabla\cdot(k_{eff}\nabla T_f)+\Phi \tag{6}$$

Where ρ_f in kg/m^3, c_f in J/(kg·K) and T_f are the density, the specific heat capacity and temperature of the fluid, respectively, k_{eff} the effective thermal conductivity, **u** is the velocity field (m/s), and Φ the viscous dissipation (W/m^3) - often negligible in low-speed flows.

The advection $\mathbf{u}\cdot\nabla T_f$ immediately reveals that the temperature field is inseparable from the velocity field: heat is carried wherever the air moves. Inside an enclosed box girder, no external wind drives this motion the flow arises entirely from buoyancy, as warmer air rises and cooler air descends in response to differential heating of the surrounding concrete walls. This mechanism is captured by incorporating a buoyancy source term into the Navier-Stokes momentum equations via the Boussinesq approximation:

$$\rho_f\left(\frac{\partial \mathbf{u}}{\partial t}+(\mathbf{u}\cdot\nabla)\mathbf{u}\right)=-\nabla p+\mu\nabla^2\mathbf{u}+\mathbf{f}_b \tag{7}$$

Where μ is the dynamic viscosity (P·s), and p is pressure (N/m^2).

To capture natural convection driven by temperature-induced density gradients inside the enclosed box girder, the buoyancy force term $\mathbf{f}_b$ is typically modeled using the Boussinesq approximation:

$$\mathbf{f}_b=\rho_0\mathbf{g}\left[1-\beta(T_f-T_0)\right] \tag{8}$$

Here, β is the thermal expansion coefficient, **g** is the gravitational acceleration vector (m/s^2), ρ_0 is the reference density at reference temperature T_0, and T_f is temperature of the fluid.

At the Rayleigh numbers characteristic of full-scale bridge sections, this buoyancy-driven flow transitions into a turbulent regime. Direct resolution of all turbulent scales is computationally prohibitive; instead, the Reynolds-Averaged Navier-Stokes (RANS) approach is adopted, introducing an effective thermal conductivity:

$$k_{\mathrm{eff}}=k_f+k_t=k_f+\frac{\mu_t c_f}{Pr_t} \tag{9}$$

Where k_f is the thermal conductivity, μ_t is the turbulent viscosity (computed via closure models such as $k-\omega$ SST or RNG $k-\varepsilon$), k_t turbulent thermal conductivity, and Pr_t is the turbulent Prandtl number (typically assumed to be approximately 0.85 for air).

Because h_c ultimately depends on the near-wall gradient, the fidelity of the result is critically sensitive to the mesh resolution at the fluid-solid interface. Wall functions - which bypass the viscous sublayer through empirical relations - are inadequate here, as buoyancy-driven recirculating flows do not conform to the log-law assumptions on which such functions rest. The mesh is therefore refined until the dimensionless wall distance satisfies equation (10), ensuring that the steep thermal gradient within the viscous sublayer is directly integrated rather than approximated.

$$y^{+} = \frac{\rho_f u_\tau y}{\mu} \approx 1 \tag{10}$$

The fluid domain does not exist in isolation: heat conducted through the concrete walls arrives at the interface and is immediately absorbed by the adjacent air. This two-way exchange is enforced through conjugate boundary conditions, requiring continuity of both temperature and heat flux across the fluid-solid interface:

$$T_f \big|_{\text{wall}} = T_s \big|_{\text{wall}} \tag{11}$$

Once the fully coupled system converges, h_c is extracted by combining the two expressions for q:

$$k_f \frac{\partial T_f}{\partial n} = k_s \frac{\partial T_s}{\partial n} \tag{12}$$

$$h_c = \frac{-k_f \left(\partial T / \partial n \right)_{\text{wall}}}{T_s - T_b} \tag{13}$$

The remaining quantity requiring careful treatment is the bulk temperature T_b. Rather than approximating it by the far-field air temperature, a mass-flow-weighted integration is performed along a line projected normally from the wall into the fluid core, filtering out near-wall boundary layer effects and numerical singularities. This ensures that the denominator in the expression for h_c reflects the true thermal driving potential at each location along the surface.

3. IMPLEMENTATION

The computational framework for determining the convective heat transfer coefficient (h_c) is executed through the following sequential pipeline:

3.1. CFD model selection

In this study, the COMSOL Multiphysics 6.4 platform is utilized to execute the proposed methodology. In coupled CFD-heat transfer simulations, the choice of a suitable flow model is paramount to obtaining reliable results [8]. Therefore, a numerical CFD model is first established and validated against benchmark experimental data [14], [15], whose geometric configurations and turbulent airflow characteristics closely match those of enclosed air cavities in real-scale bridge box girders. The temperature-dependent thermophysical properties of air are evaluated directly using COMSOL's built-in material library.

The benchmark experiment was conducted in a large-scale, differentially heated vertical cavity with dimensions of $0.75\ \text{m} \times 0.75\ \text{m} \times 1.5\ \text{m}$ (Width × Height × Depth). The high depth-to-width aspect ratio of 2.0 was specifically designed to minimize three-dimensional end-wall edge effects, thereby establishing a nearly ideal two-dimensional (2D) airflow field within the central cross-section region.

The thermal boundary conditions of the cavity were strictly controlled to induce low-turbulence natural convection:

- Vertical Walls: The left hot wall and the right cold wall were maintained at uniform, isothermal temperatures of 50 ^{o}C and 10 ^{o}C, respectively. This continuous temperature differential ($\Delta T = 40^{\circ}\mathrm{C}$) in air yields a high fluid-structure thermal Rayleigh number of $Ra = 1.58\times10^{9}$, driving the buoyancy-induced flow into a low-level turbulent regime.

- Horizontal Walls: The top and bottom horizontal walls were highly insulated to approximate ideal adiabatic conditions.

Throughout the experiment, highly accurate sensors and measurement techniques were systematically deployed at multiple internal coordinates to capture the symmetrical distributions of the velocity vectors, local wall shear stresses, sharp near-wall thermal boundary layer profiles, and the resulting local/average Nusselt numbers (*Nu*) providing a high-resolution dataset for CFD validation.

The computational mesh was generated using the physics-controlled meshing sequence in COMSOL Multiphysics and was verified to ensure no inverted or low-quality elements existed. The boundary layer mesh was properly resolved to satisfy the dimensionless wall distance criteria $y^{+} \approx 1$ as specified in Equation (10). Furthermore, a grid independence test was conducted across four COMSOL built-in mesh densities: *Normal, Fine, Finer,* and *Extra fine*. As depicted in Figure 1, the temperature profiles obtained from the *Finer* and *Extra fine* meshes are practically identical across both the thermal boundary layer and the core domain, with a relative discrepancy below 0.8% at all control points. Consequently, the *Finer* mesh configuration was adopted for subsequent simulations to strike an optimal balance between numerical precision and computational efficiency. In this selected mesh, the boundary layer consists of a first layer thickness of 0.00018 m with a stretching factor (growth rate) of 1.2.

To evaluate the performance of different turbulence closure models in predicting buoyancy-driven flows within enclosed spaces, both the standard $k-\epsilon$ and the Shear Stress Transport (SST) $k-\omega$ models were tested against the benchmark experimental data. The comparative analysis indicated that the SST $k-\omega$ model exhibits superior accuracy in capturing the low-speed fluid motion and the sharp thermal gradients within the thin boundary layers near the solid walls. Consequently, the SST $k-\omega$ framework is selected for the subsequent real-scale bridge girder simulations to ensure consistent and reliable predictions of the convective heat transfer coefficients.

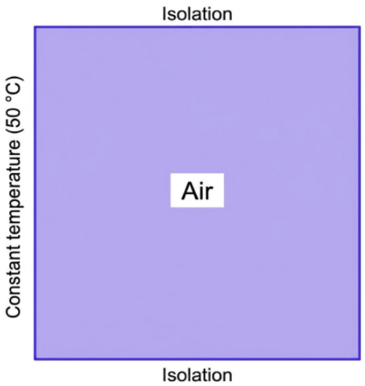

(a)

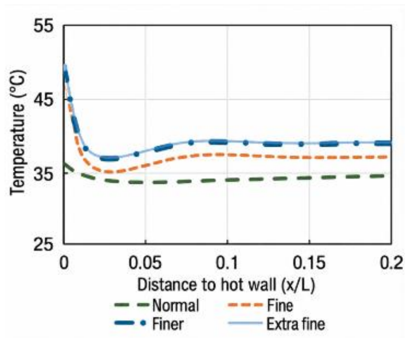

(b)

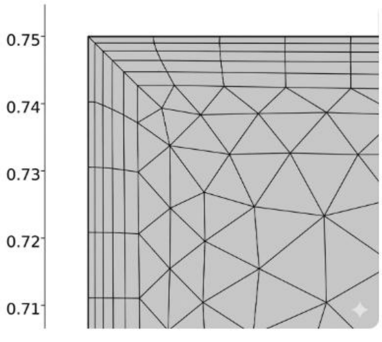

(c)

Figure 1. (a) Analysis domain, (b) Grid-independent test, (c) Mesh structure near walls.

Figure 2 and Figure 3 demonstrate good agreement in the temperature distribution across the entire domain, particularly within the near-wall boundary layers. Based on these validated results, the proposed numerical approach is subsequently applied to full-scale bridge structures.

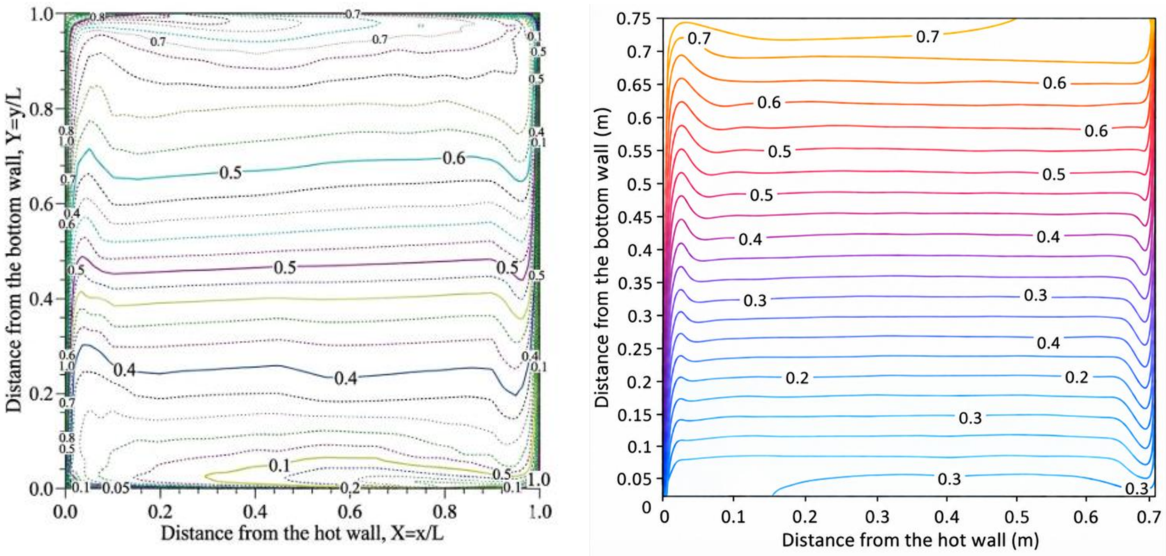

(a) Experiment *(b) Simulation*

Figure 2. Comparing the temperature distribution in whole domain.

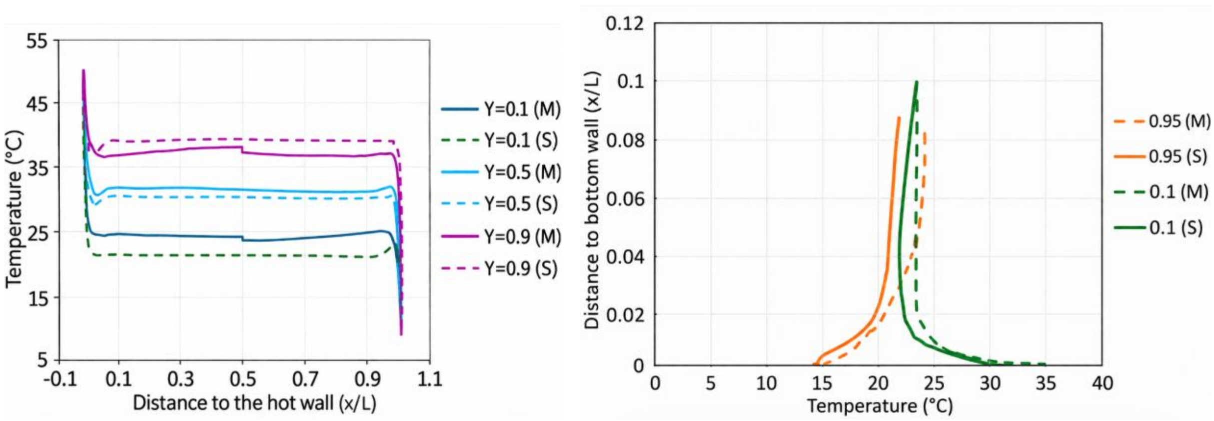

Figure 3. Comparing the temperature distribution - (a) in X direction and (b) Y direction near bottom wall. M: measured, S: Simulated.

3.2. Real structure simulation and field verification

The 2D CFD simulation in this study is conducted across six bridge sections, as illustrated in Figure 4. At these sections, temperatures are monitored using thermocouples positioned according to Figure 5a. Specifically, thermocouples #3, #6, #9, #12, #15, and #18 capture the concrete temperatures adjacent to the interior surfaces, whereas thermocouple #20 records the ambient air temperature. Temperature data are continuous with a logging interval of 5 minutes. The computational domains for the CFD simulation encompass the air volume inside the box girders. Time-dependent temperature profiles, derived from the aforementioned interior-surface thermocouples, are prescribed as the boundary conditions. Finally, the air temperature data recorded by thermocouple #20 are utilized to validate the numerical simulation results (Figure 5b).

The flow model used in this simulation is *SST k-ω* because this model is capable of capturing the flow velocity and temperature near the wall as shown in (3.1). The mesh for each domain is built fine enough so that the dimensionless wall distance $y^+ \approx 1$ and the spatial resolution was rigorously verified through the aforementioned grid independence study.

Figure 6 shows the distribution of temperature and velocity of fluid in the analysis domain. Figure 7, Figure 8 and Figure 9 demonstrate a high degree of correlation between the measured (M) and simulated (S) ambient air temperatures inside the box girder across all six evaluated sections. The numerical model successfully captures not only the daily cyclic temperature profiles but also the exact timing and magnitudes of the maximum peaks and minimum troughs. While the experimental data (M) exhibit minor high-frequency fluctuations due to sensor sensitivity and localized air turbulence, the CFD simulation (S) effectively predicts the core thermodynamic trend. Furthermore, the strong agreement maintained across diverse time spans and different seasonal conditions underscore the robustness and reliability of the developed numerical framework.

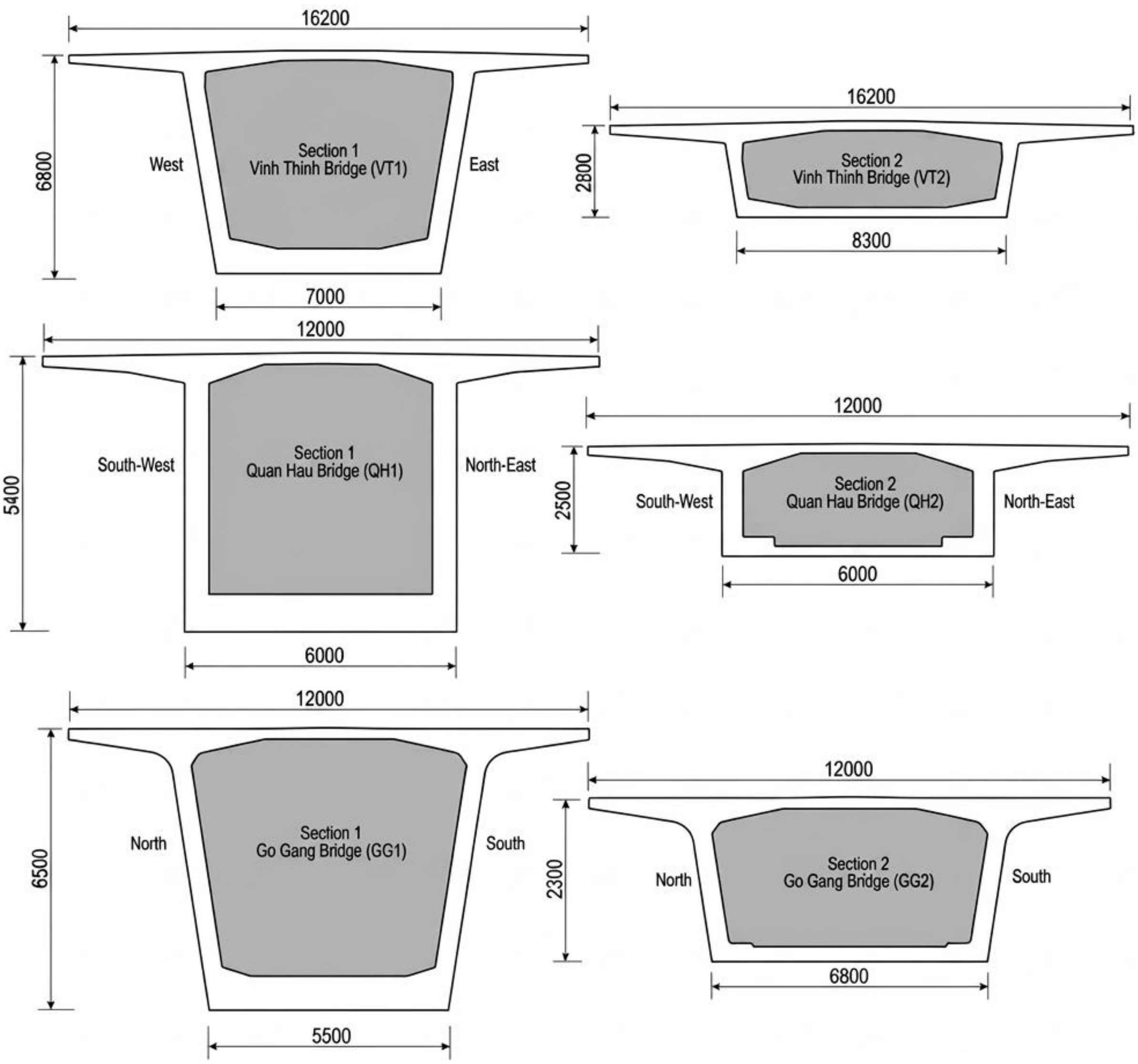

Figure 4. Bridge sections and CFD simulation domains.

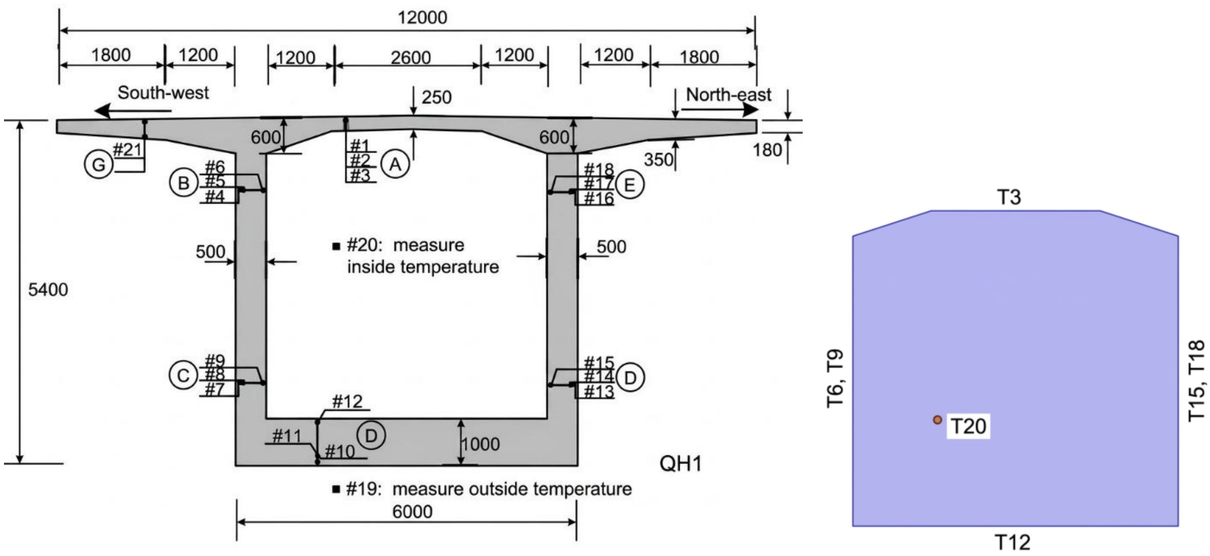

(a) Layout of thermocouple in bridge section *(b) Temperature boundary condition in simulation*

Figure 5. (a) Layout of thermocouple in bridge section; and (b) Temperature boundary condition in simulation.

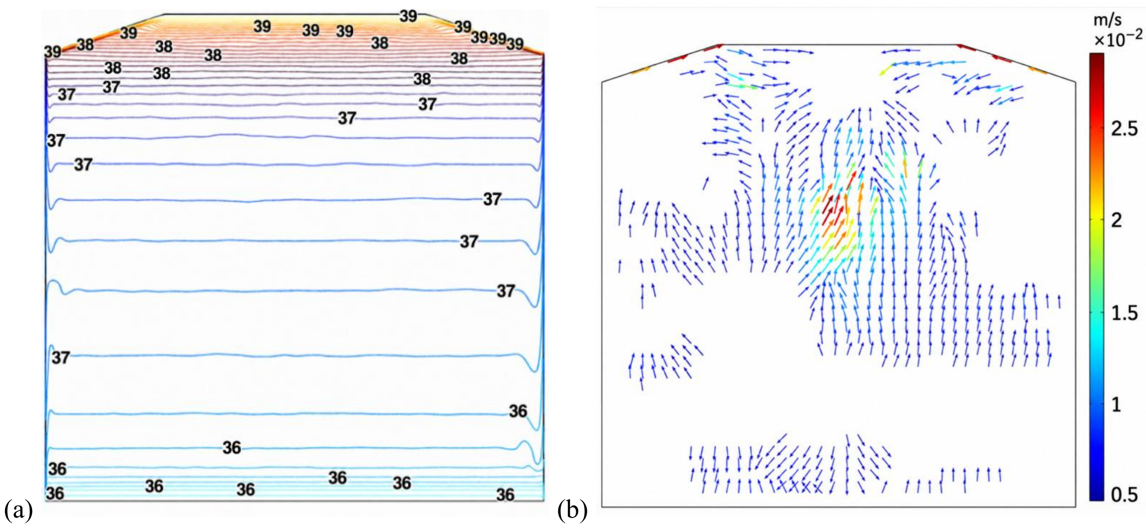

Figure 6. Distribution of (a) temperature; and (b) velocity of air inside box girder of section QH1.

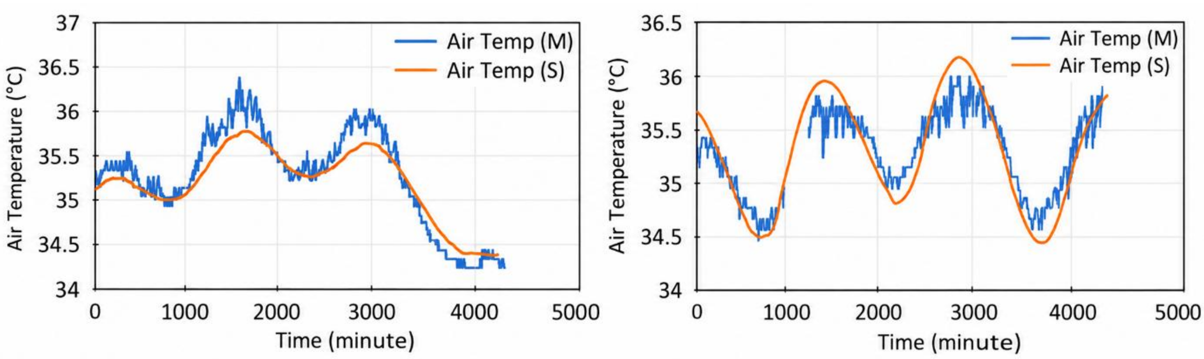

(a) VTI from 21/06/2022 to 23/06/2022 *(b) VT2 from 01/06/2023 to 03/06/2023*

Figure 7. Comparing measured (M) and simulated (S) air temperature inside box girder.

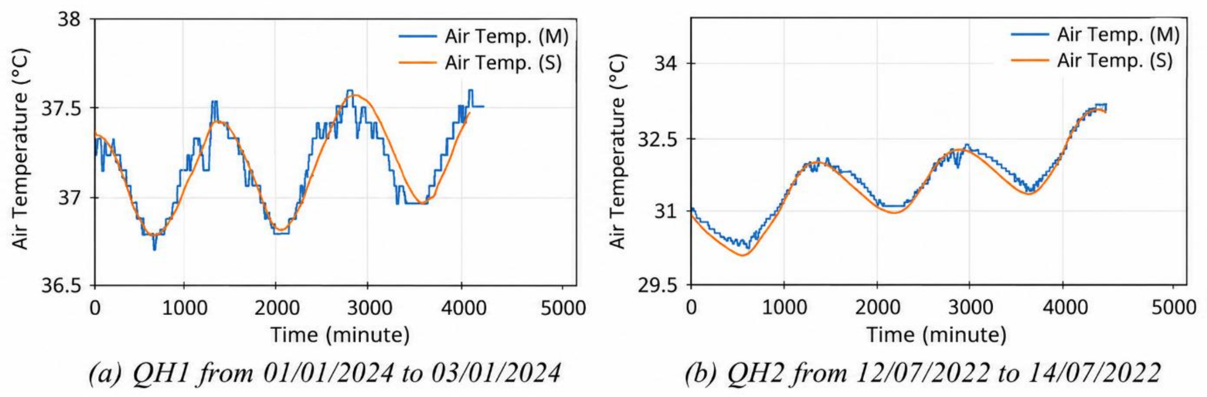

Figure 8. Comparing measured (M) and simulated (S) air temperature inside box girder.

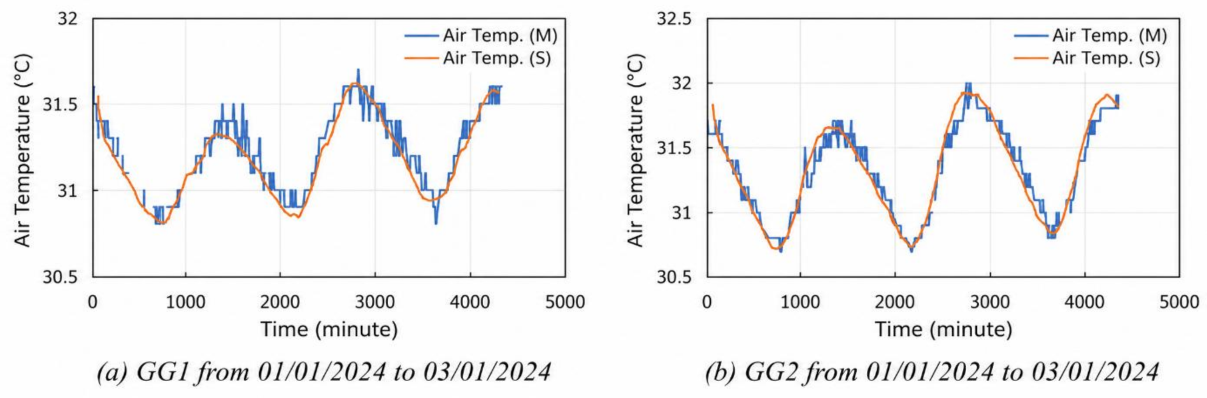

Figure 9. Comparing measured (M) and simulated (S) air temperature inside box girder.

3.3. Local CHTC Extraction

Rather than relying on empirical values, the local convective heat transfer coefficient (hc) inside the box girder is dynamically extracted from the coupled CFD and heat transfer simulation via COMSOL Multiphysics using the following formulation:

$$h_c = \left| \frac{k_{mean} \cdot \nabla T}{T_{wall} - T_b} \right| \tag{14}$$

where k_{mean} is the thermal conductivity of air, ∇T is the temperature gradient magnitude at the boundary, and T_{wall} is the local solid surface temperature (in COMSOL $T_{wall} = ht.T_{var}$).

To account for the spatial fluid flow variations without thermal boundary layer interference, the local bulk temperature (T_b) is dynamically computed using non-local coupling operators. This algorithm projects a normal integration line from the wall into the core fluid domain spanning a distance of $\pm B_2$, executing a mass-flow-weighted integration:

$$T_b = \frac{\int_{-B_2}^{B_2} \mathcal{I}(s) \cdot \left[u(s) \cdot T(s) \right] ds}{\int_{-B_2}^{B_2} \mathcal{I}(s) \cdot u(s) ds} \tag{15}$$

Here, $u(s)$ and $T(s)$ are the localized velocity and temperature fields, while $\mathcal{I}(s)$ is an indicator function filtering out non-fluid domains and numerical singularities (NaN). Supported by a highly refined boundary layer mesh ($y^+ \approx 1.6 \div 2.0$), this approach ensures an exceptionally accurate, grid-independent estimation of the local thermal behavior inside the structure.

For instance, Figure 10 and Figure 11 illustrate the variation of CHTCs of the interior surfaces across sections QH1, GG1, VT2, and QH2. In coupled fluid-structure simulations, these localized values are highly susceptible to numerical singularities; transient fluid-solid thermal gradients can trigger momentary, extreme fluctuations when local air velocities approach stagnation points or during air-cell inversion phases, causing the spikes observed in the raw computational profiles. To establish a representative thermal baseline without artificial filtering, a descriptive statistical framework is implemented (Table 1). While the arithmetic average is exceptionally sensitive to outliers, the median (*M*) remains robust. The tight convergence between these two indicators demonstrates that the temporal density of numerical spikes is negligible relative to the massive dataset. Consequently, the symmetric core distribution allows the narrow boundaries of the first (*1Q*) and third (*3Q*) quartiles to safely isolate numerical artifacts while preserving the predominant physical regime of the internal natural convection.

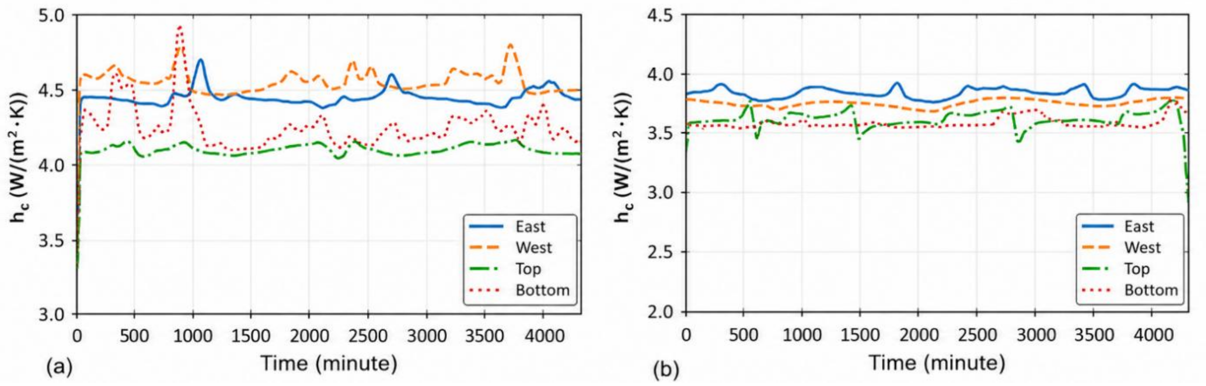

Figure 10. Calculated CHTC for (a) QH1 and (b) GG1 sections.

The average h_c values presented in Table 1 are calculated by considering the weighted influence of the convective heat transfer coefficient alongside the respective length of each edge relative to the entire section perimeter, as formulated below:

$$h_{c\_average} = \frac{\sum h_{ci} \cdot L_i}{\sum L_i} \tag{16}$$

An interesting physical trend observed from the extracted parameters (Table 1) indicates that sections with smaller geometric dimensions and more square-like aspect ratios consistently exhibit higher h_c values. This behavior aligns with the fundamental principles of confined natural convection. In smaller enclosures, the reduced distance between the core air mass and the solid boundaries inherently steepens the localized temperature gradients (dT/dx), thereby intensifying the convective heat flux. Furthermore, square-like cross-sections facilitate the formation of symmetric, unobstructed convective cells. Unlike slender or highly eccentric geometry where flow stagnation typically occurs near narrow corners, the well-proportioned space sustains robust air circulation velocities, which directly elevates the convective heat transfer coefficients (h_c).

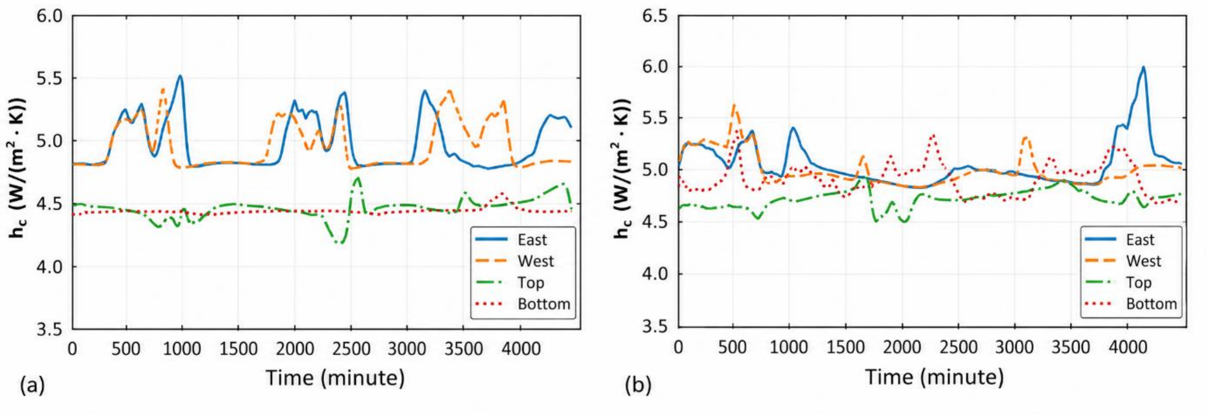

Figure 11. Calculated CHTC for (a) VT2 and (b) QH2 sections.

Table 1. Statistical summary of representative h_c values ($W \cdot m^{-2} \cdot K^{-1}$) for interior surfaces across different structural sections.

Section	Surfaces				Average
	Top	Bottom	West	East	
VT1	3.84	3.82	4.00	3.96	3.92
VT2	4.40	4.48	4.80	4.79	4.60
QH1	4.10	4.22	4.43	4.54	4.32
QH2	4.78	4.92	5.04	4.98	4.90
GG1	3.62	3.58	3.84	3.77	3.71
GG2	4.20	4.19	4.45	4.35	4.25

4. VALIDATION

The calculated h_c values are applied to simulate the thermal behavior of bridge sections with different configurations across different time spans. Within the COMSOL numerical models, which utilize the "Heat Transfer in Solids" module, the boundary conditions are governed by the field-measured temperatures from the outer surface thermocouples (e.g., #1, #7, and #10). Crucially, the convective heat exchange inside the cell is simulated between the interior concrete surfaces and the enclosed air domain, where the internal air temperature is driven by the actual experimental data recorded directly by thermocouple #20. This convective process is governed by the previously derived weighted h_c values. The simulation was validated against temperature measurements from the sensors installed inside the concrete (e.g., #2, #3, #8, #11, #12). Figure 12 illustrates the simulation model for thermal behavior of bridge section with using the calculated h_c.

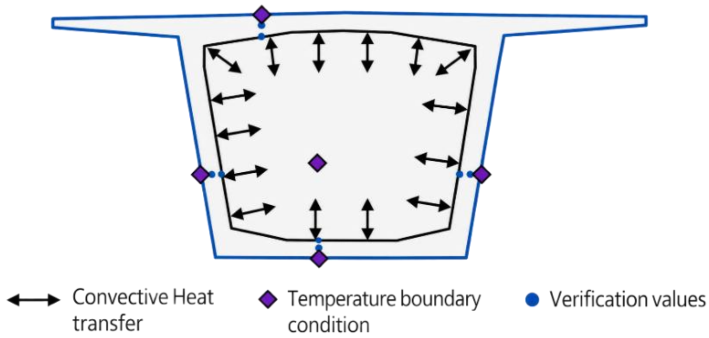

Figure 12. Schematic diagram of the heat transfer model for the concrete cross-section.

The key thermal properties of concrete used in the simulation - thermal conductivity of $1.8\ \mathrm{W/(m\cdot K)}$, density of $2400\ \mathrm{kg/m^3}$, and specific heat capacity of $880\ \mathrm{J/(kg\cdot K)}$ - were adopted from [16]. Figure 13, Figure 14 and Figure 15 illustrate the comparison between the measured and simulated temperatures across various structural sections and time frames. The high degree of convergence between the numerical and experimental curves confirms that the simulation models are fully validated. Consequently, the obtained h_c values can serve as reliable reference convective heat transfer coefficients (CHTC) for evaluating the thermal behavior of concrete box girder structures with similar geometric configurations.

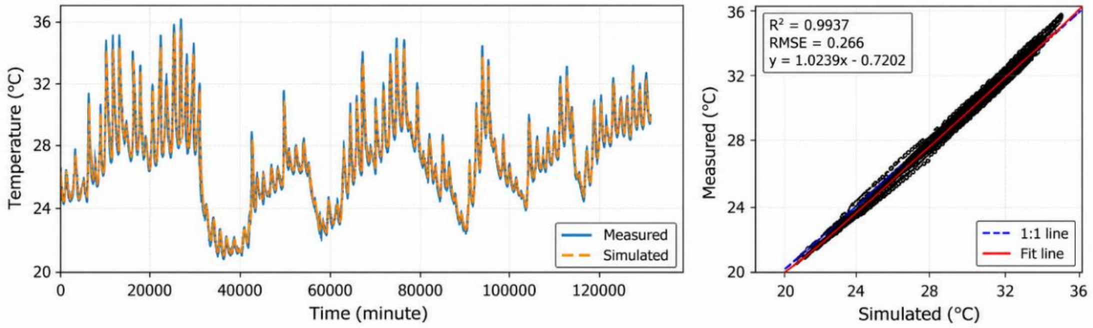

(a) time history comparison *(b) parity plot*

Figure 13. Comparison between measured and simulated temperatures at QH1, thermocouple #8 (web slab) from 01/01 to 31/03/2024.

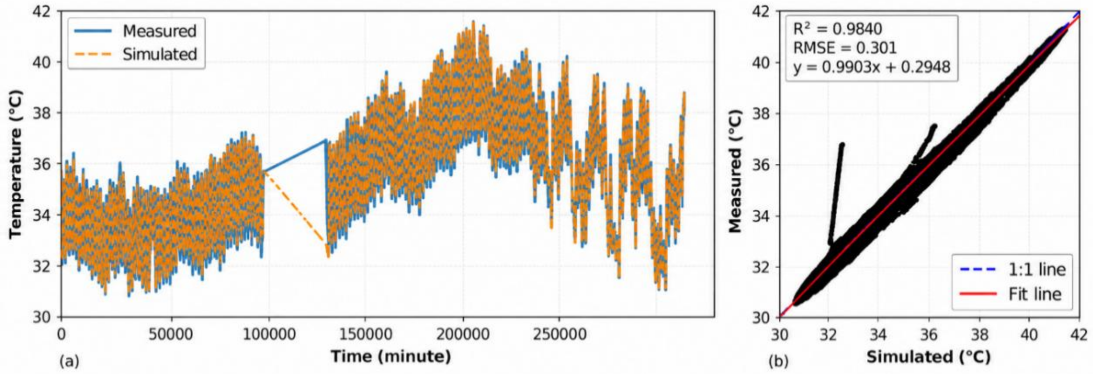

(a) time-history comparison *(b) parity plot*

Figure 14. Comparison between measured and simulated temperatures at GG1, thermocouple #3 (top slab) from 01/01 to 30/06/2024.

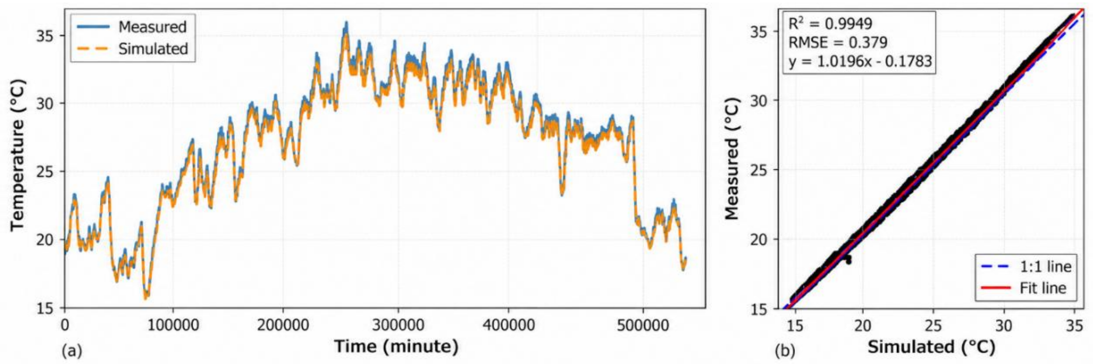

(a) time-history comparison *(b) parity plot*

Figure 15. Comparison between measured and simulated temperatures at VT2, thermocouple #12 (bottom slab), from 01/01 to 31/12/2022.

5. CONCLUSION

This paper presents a CFD-based methodology for determining the convective heat transfer coefficient (h_c) on the internal surfaces of concrete box girder bridges, addressing the limitations of traditional empirical formulas. Implemented within the COMSOL Multiphysics platform, the framework focuses on the internal air cavity by coupling turbulent fluid flow with heat transfer in the fluid domain. The numerical framework is validated against both a benchmark laboratory experiment and field-measured temperature data from six full-scale bridge cross-sections across diverse geometric configurations and seasonal conditions.

The results demonstrate that hc values on internal surfaces are not constant as assumed by Kehlbeck's empirical formula, but vary spatially and temporally depending on the geometry of the enclosed cross-section. Extracted h_c values range from approximately 3.71 to 4.9 $W \cdot m^{-2} \cdot K^{-1}$ across the studied sections, with vertical web surfaces consistently yielding higher coefficients than horizontal top and bottom slabs. A clear physical trend is confirmed: sections with smaller dimensions and more square-like aspect ratios exhibit higher h_c values, attributable to steeper near-wall temperature gradients and more robust natural convection cells.

The validated hc values are subsequently applied to simulate the thermal behavior of bridge structures in full monthly time spans. The strong agreement between measured and simulated concrete temperatures confirms the reliability of the derived coefficients as practical reference values for thermal analysis of concrete box girder bridges with similar geometric configurations.

The findings of this study highlight the importance of geometry-specific h_c values in achieving accurate thermal predictions, which are critical for evaluating temperature-induced stresses and cracking in box girder bridges. Future work will focus on non-dimensionalizing the results through Nusselt-Rayleigh number correlations to establish generalized empirical relations applicable to a wider range of cross-sectional geometries.

ACKNOWLEDGEMENT

This research is funded by University of Transport and Communications (UTC) under grant number T2026-XD-005.

REFERENCES

[1]. R. A. Imbsen, R. A. Vandershaf, Thermal Effects in Concrete Bridge Superstructure, NCHRP Report 276, 1985.

[2]. T. T. Tung, Evaluation of the effectiveness of cantilever construction technology for large-span prestressed reinforced concrete bridges in Vietnam and proposal for improvement solutions, Report on research results of a MOT project, Code: DT183057, 2019. (in Vietnamese).

[3]. J. H. Lienhard, A Heat Transfer Textbook, fifth ed., Courier Dover Publications, 2019.

[4]. J. P. Holman, Heat Transfer, tenth ed., McGraw-Hill, 2010.

[5]. D. N. Quang, H. N. Cuong, Determination of convective heat transfer coefficients for exterior surfaces of concrete bridge box girders using CFD conjugate heat transfer simulation, Transport and Communications Science Journal, 76 (2025) 333-347. https://doi.org/10.47869/tcsj.76.3.11

[6]. M. M. Elbadry, A. Ghali, Temperature variations in concrete bridges, Journal of Structural Engineering, 109 (1983) 2355-2374. https://doi.org/10.1061/(ASCE)0733-9445(1983)109:10(2355)

[7]. D. N. Quang, Determining the convective heat transfer coefficient of inside surfaces of concrete box bridge girders, Journal of Construction, 6 (2025). (in Vietnamese).

[8]. H. Montazeri, B. Blocken, D. Derome, J. Carmeliet, J. L. M. Hensen, CFD analysis of forced convective heat transfer coefficients at windward building facades: Influence of building geometry, Journal of Wind Engineering and Industrial Aerodynamics, 146, 102-116. https://doi.org/10.1016/j.jweia.2015.07.007

[9]. M. T. Kahsay, G. T. Bitsuamlak, F. Tariku, CFD simulation of external CHTC on a high-rise building with and without façade appurtenances, Building and Environment, 165 (2019) 106350. https://doi.org/10.1016/j.buildenv.2019.106350

[10]. S. R. Delaforce, E. R. Hitchin, D. M. T. Watson, Convective heat transfer at internal surfaces, Building and Environment, 28 (1993) 211-220. https://doi.org/10.1016/0360-1323(93)90054-7

[11]. G. V. Kuznetsov, A. E. Nee, Conduction, convection, and radiation in a closed cavity with a local radiant heater, Frontiers in Heat and Mass Transfer, 10 (2018) 1-9. https://doi.org/10.5098/hmt.10.26

[12]. A. Bejan, Convective Heat Transfer, John Wiley & Sons, Inc., 2013.

[13]. H. B. Awbi, A. Hatton, Natural convection from heated room surfaces, Energy and Buildings, 30 (1999) 233-244.

[14]. Y. S. Tian, T. G. Karayiannis, Low turbulence natural convection in an air filled square cavity Part I: The thermal and fluid flow fields, International Journal of Heat and Mass Transfer, 43 (2000) 849-866.

[15]. Y. S. Tian, T. G. Karayiannis, Low turbulence natural convection in an air filled square cavity Part II: The turbulence quantities, International Journal of Heat and Mass Transfer, 43 (2000) 867-884.

[16]. N. D. Quang, Final Report on the Research Project: Investigation into Temperature Distribution in Reinforced Concrete Box Girder Highway Bridges, DT214005, 2022. (in Vietnamese).